Supporting Information for

Tunable 3D hierarchical Ni_3S_2 superstructures as efficient and ultrastable bifunctional electrocatalysts for both H_2 and O_2 generations

Lingyou Zeng, Kaian Sun, Zhichao Yang, Shengli Xie, Zhi Liu, Yanju Chen, Yaqing Liu, Jinchong Zhao, Yunqi Liu* and Chenguang Liu*

State Key Laboratory of Heavy Oil Processing, Key Laboratory of Catalysis, China University of Petroleum (East China), Qingdao, 266580, P. R. China.

Corresponding author: liuyq-group@upc.edu.cn; cgliu@upc.edu.cn

The supporting information includes two sections: I More experimental Details; II Additional Data and Figures.

I. More experimental Details

I.1 Chemical etching method

Chemical etching is generally used in the industrial metal removal to acquire components that cannot be machined easily throughout conventional machining techniques. Normally, a strong chemical bath with specified temperature is conducted to mental surfaces, where metal cations are released from the metal substrates into the solution to obtain specific shapes.[1-3] Taking the merit of this method, we speculate this synthesis of 3D nanostructures could be achievable in a hydro/solvo-thermal solution, due to the exfoliated metal ions may nucleate into crystalline grain.[4] Driven by the energy fluctuation, the as-formed grains may further grow into secondary architectures of target products.[5-7] Hence the chemical etching in a hydro/solvo-thermal process may ultimately bring about objective materials with peculiar structural morphologies, high surface active areas, and good adhesion to the metal substrates, thus giving the materials with particular functionality for widespread applications, such as electrocatalysis.

In this work, Nickel foam here acts dual roles of nickel ions sources and supporting frameworks, in which Ni atoms are dissolved into cations derivatives when attacked via chemical etching, further reacting with thiourea (Tu), the sulfide ions source, to grow 3D Ni_3S_2 superstructures.

I.2 IR correction

To fairly compare the performance of various catalysts, all the polarization curves were corrected for ohmic losses throughout the system, which include the wiring, substrate, catalyst material, and solution resistances. All these resistances constitute the series resistance (R_s) of the measurement. The R_s can be obtained from an EIS Nyquist plot as the first intercept of the main arc (corresponding to the electrode-electrolyte interface) with the real axis. For all measurements, the values of Rs are low and consistent. Then the IR-corrected data is given by $E_{Corrected} = E_{Raw}\text{-}IR_s$.

I.3 Electrochemical active surface area (ECSA)

The active surface area of each catalyst was estimated from their electrochemical capacitances, which can be measured using a simple cyclic voltammetry method. We measured the currents in a narrow potential window that no faradic processes were observed, thus the currents should be mostly, if not only, due to the charging of the double layer, which is expected to be linearly proportional to the active surface area. By plotting the capacitive currents (ΔJ, J_{anodic} - $J_{cathodic}$) against the scanning rate and following with a linear fit, the double layer capacitance (C_{dl}) can be estimated as half of the slope (see Fig.S1 for an example of NF-Ni_3S_2/NF). The C_{dl} can be further converted into ECSA using the specific capacitance value for a standard with 1 cm^{-2} of real surface area. The specific capacitance for a flat surface is normally between 0.02-0.06 mF cm^{-2}. Note Ni foam was used as the support its capacitance value is much larger than that of a flat surface. Therefore, here Ni foam was considered as the standard. The ECSA of each catalyst can be calculated according to:

$$A_{ECSA} = \frac{C_{dl-catalyst}\ (mF\ cm^{-2})}{C_{dl-Ni\ foam}\ (mF\ cm^{-2})\ per\ ECSA\ cm^{-2}}$$

Taking NF-Ni_3S_2/NF as an example, upon the hydrogen evolution reaction, the ECSA of NF-Ni_3S_2/NF can be calculated as:

$$A_{ECSA}^{NF-Ni_3S_2/NF} = \frac{99.2\ mF\ cm^{-2}}{3.8\ mF\ cm^{-2}\ per\ ECSA\ cm^{-2}} = 26.1\ cm^2_{ECSA}$$

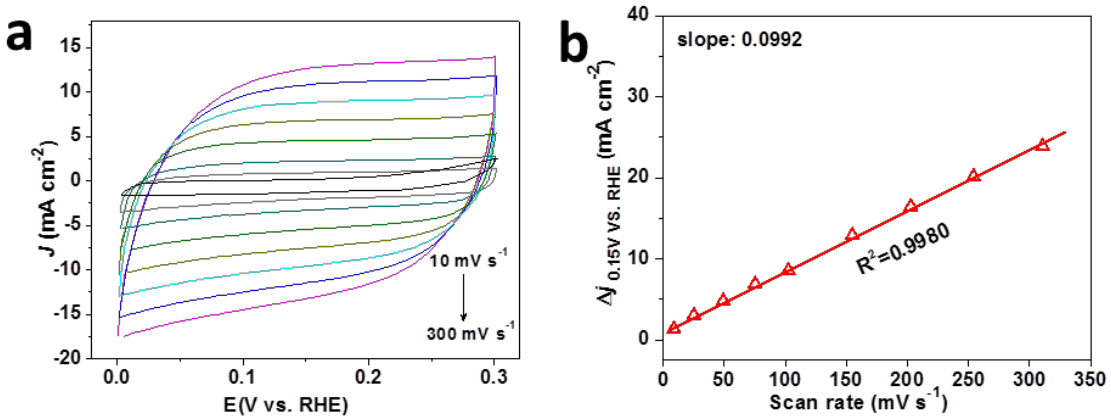

Figure S1. Electrochemical capacitance measurements for the estimation of the relative elec-

trochemical active surface area of NF-Ni_3S_2/NF upon HER. (a) Cyclic voltammograms in the region of 0-0.3 V vs RHE. (b) The differences in current density at 0.150 V vs RHE plotted as a function of scan rate fitted to a linear regression, where the slope is twice C_{dl}.

I.4 Determination of Faradaic efficiency

The Faradic efficiency of a catalyst in HER or OER is defined as the ratio of the amount of H_2 or O_2, respectively, evolved during the experiments to the amount of H_2 or O_2 expected based on theoretical considerations. So, to measure the Faradic efficiency of, for example, HER we carried out the following experiment. We collected the evolved H_2 gas by water drainage method, and then calculated the moles of H_2 generated from the reaction with an ideal gas law. The purity of the generated gas was confirmed by gas chromatography (GC) analysis. As for the theoretical value, we assumed that 100% current efficiency occurs during the reaction, which means only the HER process takes place at the working electrode. We can then calculate the theoretical amount of H_2 evolved by applying the Faraday law, which states that the passage of 96485.4 C charge causes 1 equivalent of reaction.

I.5 Turnover frequency (TOF) calculations

Cyclic voltammetry (CV) curves were measured at 0.05 V s^{-1} in phosphate buffered saline solution (PBS, pH = 7.0). Then the absolute components of the voltammetric charges (ca-thodic and anodic) reported during a single measurement was added. The quantity of active species (*N*) is calculated according to the formula:

$$N = \frac{Q}{2F} = \frac{i \cdot t}{2F} = \frac{i \cdot V/u}{2F}$$

where Q is the cyclic voltammetric charge capacity obtained by integrating the CV cures, F is the Faradic constant (96485 C mol^{-1}), i is the current density (A), V is the voltage (v) and u is the scanning rate (V s^{-1}).

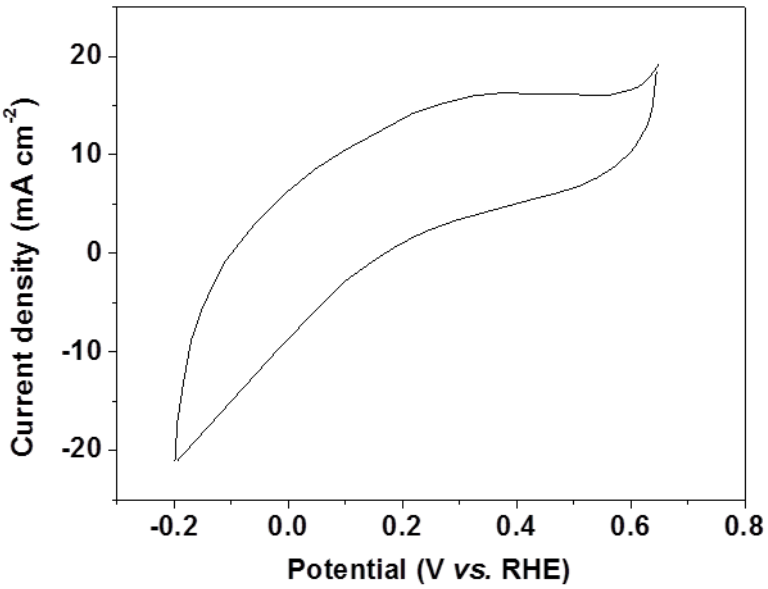

Figure S2. CV curve of NF-Ni_3S_2/Ni foam in PBS solution (pH = 7.0) at a scan rate of 50 mV s^{-1}

The TOF values are calculated via the following equation:

$$TOF = \frac{|j|A}{mFN}$$

where $|j|$ is the current density at a fixed voltage during the LSV measurement in 1.0 M solu-

tion, A stands for the area of the electrode (0.5 cm^{-2}) and F is the Faradic constant (96485 C mol^{-1}). N represents the quantity of active sites. A factor of $1/m$ is introduced, taking into ac-count that m electrons are consumed to form one H_2 or O_2 molecule from water (i.e. 2 elec-trons for hydrogen evolution reaction and 4 electrons for oxygen evolution reaction).

II. Additional Data and Figures

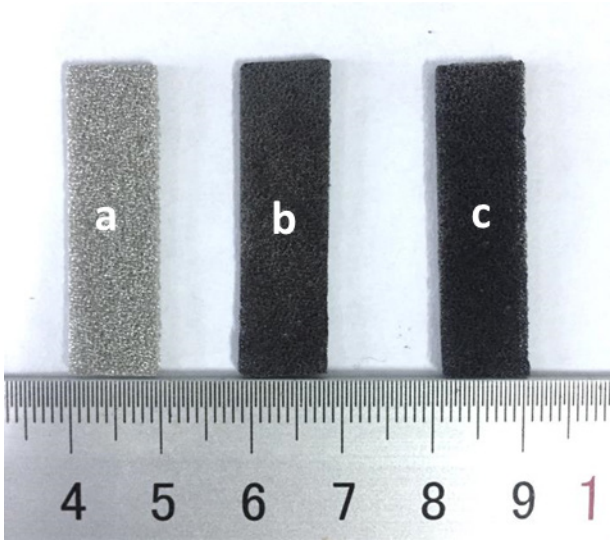

Figure S3. The digital images of (a) pure NF, (b) RA-Ni_3S_2/NF, (c) NF-Ni_3S_2/NF

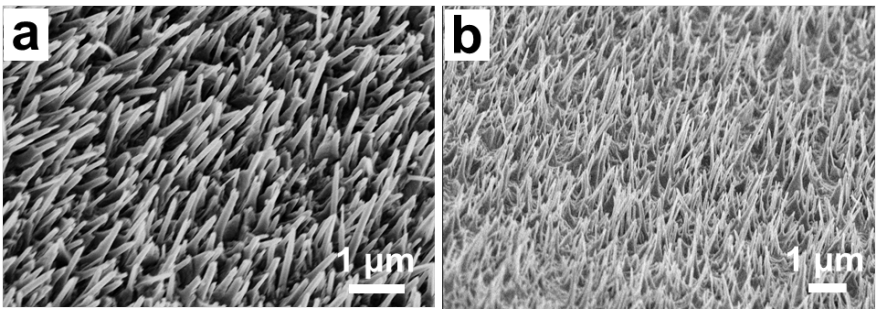

Figue S4. Additional SEM images of RA-Ni_3S_2/NF

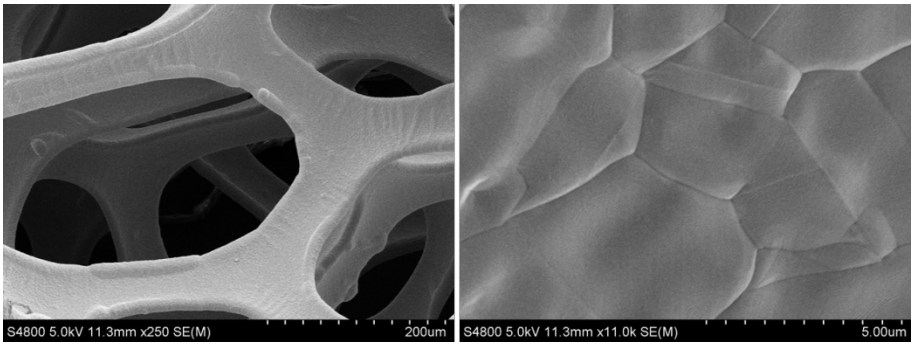

Figure S5. SEM images of bare Ni foam. The SEM image reveals the smooth surface of bare Ni foam.

Formation mechanism analysis of Ni_3S_2 nanoforests

To clarify the formation mechanism of Ni_3S_2 nanoforest supported on Ni foam, SEM, and XRD are used to characterize the intermediates collected at different reaction stages (Figures S6-9). After the reaction of Ni foam with thiourea and EDA for 10 min, the color of the Ni foam rapidly changes from silver gray to gray black, suggesting the possible reaction of Ni with S ions in solution. SEM (Figure S6b) reveals that the spherical nanoparticles are produced. In addition to the peaks of Ni, weak peaks attributed to the rhombohedral phase of NiS (JCPDS 77-1624) can be observed in XRD pattern (Figure S7). When the reaction proceed for 30 min, some nanoparticles on Ni foam become short nanorods on substrate (Figure S6c). Along with further reaction for 1 h 30 min, nanowires with branching structures are found (Figure S6d), and the associated XRD pattern (Figure S7) confirm the existence of rhombohedral NiS and hexagonal Ni_3S_2, suggesting the growth of small rhombohedral NiS branches on hexagonal Ni_3S_2 trunks may proceed via phase-transition induced branching mechanism, similar to that of CdTe tetrapods with wurtzite-phase branches and tetrahedral zinc-blende core.[8] When the reaction time is increased to 3 h, the XRD signals of rhombohedral NiS disappear, suggesting the totally transformation from rhombohedral NiS to hexagonal Ni_3S_2. Such phase transformation is previously reported and explained by Li group.[9] This process can be due to that the continuous supply of Ni ions, released from Ni substrate by the induced role of EDA,[10] provide nickel source for the growth of trees. Defects on the surfaces of both the trunks and branches can provide nucleation sites for the growth of both the trunks and branches.[11] The disappearance of some small nanowires and sampling can be attributed to Ostwald ripening process.[12]

Based on these above-mentioned results and discussion, we propose the possible growth mechanism of Ni_3S_2 nanoforest/Ni foam (Figure S9). The mechanism seems to the amine-assisted self-catalyzed NiS nanowire growth, the following phase-induced branching of Ni_3S_2 on NiS nanowires, accompanying phase-transfer reaction from rhombohedral NiSe to hexagonal Ni_3S_2, the sequential self-catalyzed growth of hierarchical branches and the final formation of treelike architectures. Ostwald ripening process may accompany the growth

process.

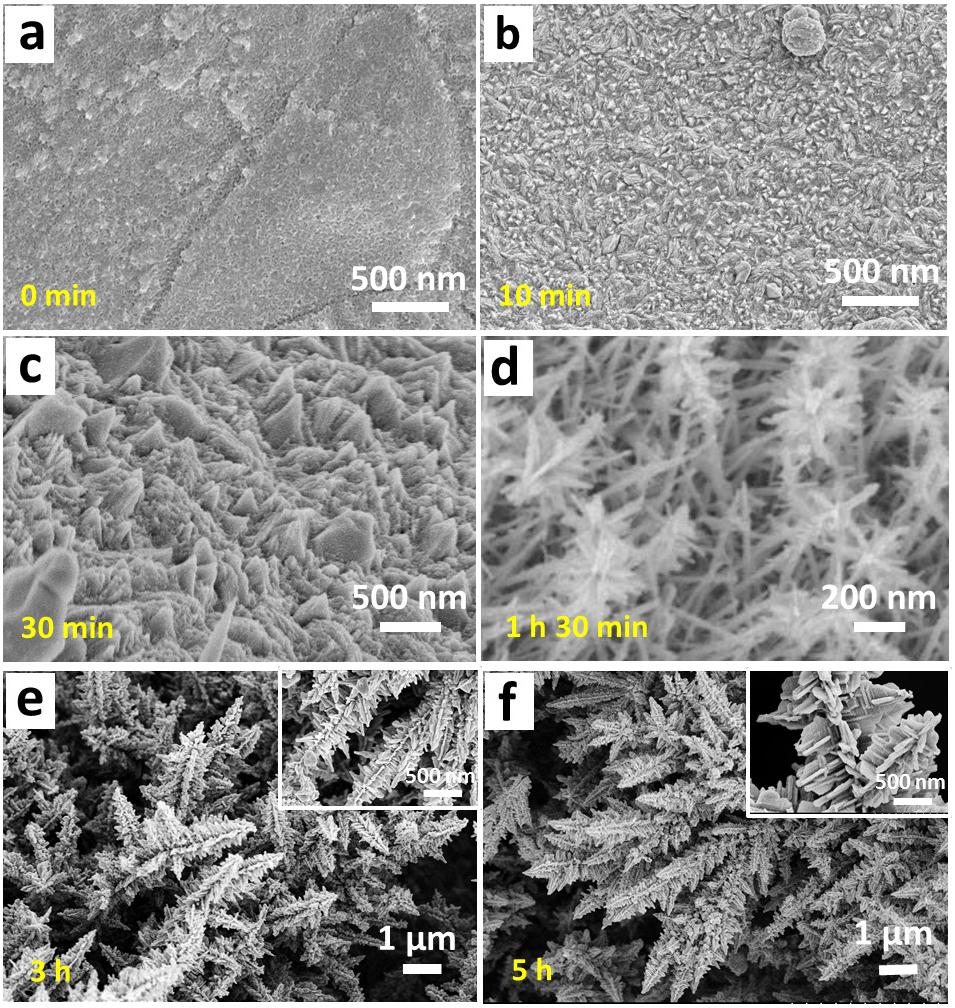

Figure S6. SEM images of the intermediates collected after the reaction proceeded for different reaction time.

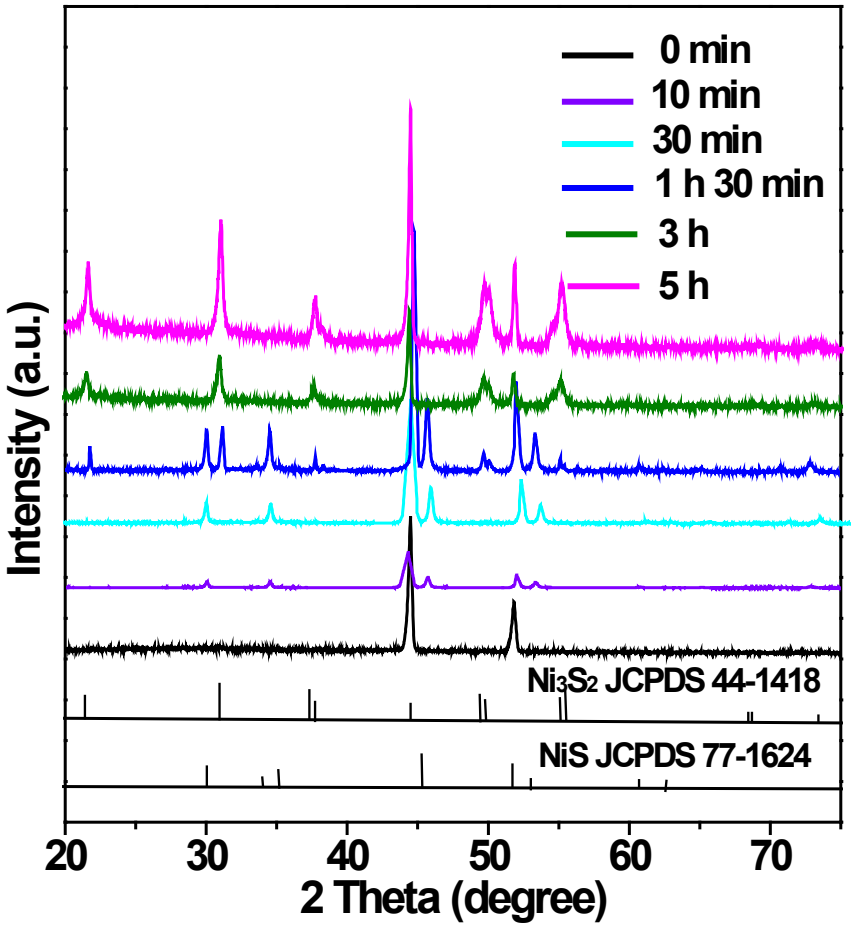

Figure S7. XRD patterns of the intermediates collected after the reaction proceeded for different time.

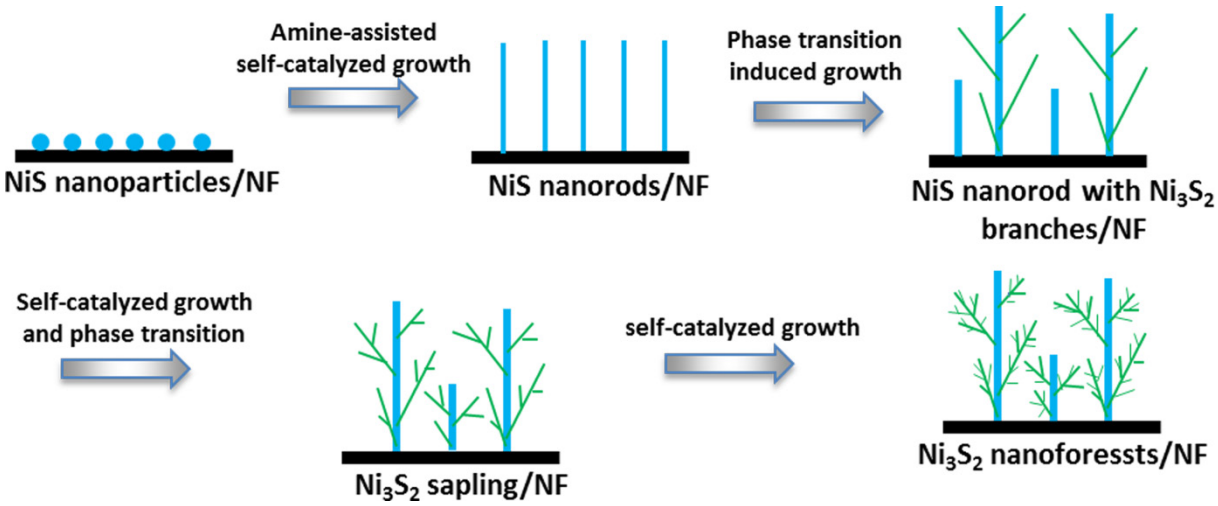

Figure S8. Scheme illustrating for the formation process of Ni_3S_2 nanoforests on Ni foam

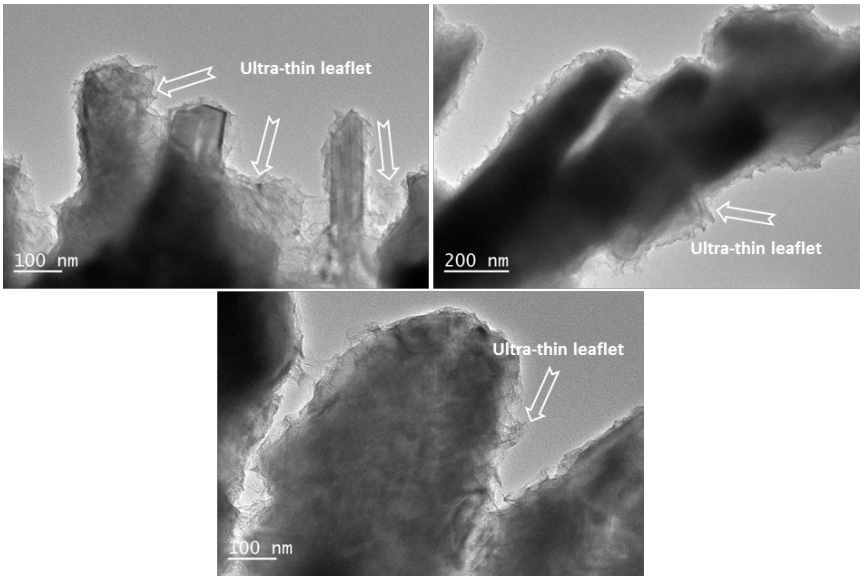

Figure S9. Additional TEM images of NF-Ni_3S_2/NF. In the TEM images, the branched structure is enveloped in a thin layer of ultrathin nanosheets, which possibly deliver unexpectedly excellent electrochemical catalytic performance due to the abundant electroactive sites.

Brunauer-Emmett-Teller (BET) analysis

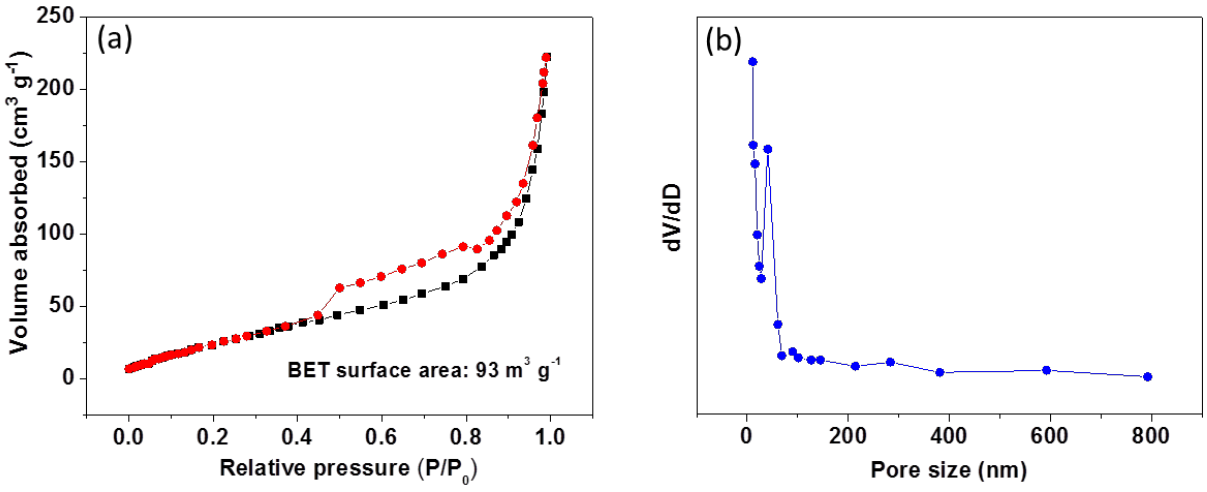

Figure S10. (a) N_2 adsorption isotherm and (b) the corresponding pore size distribution of NF-Ni_3S_2/NF

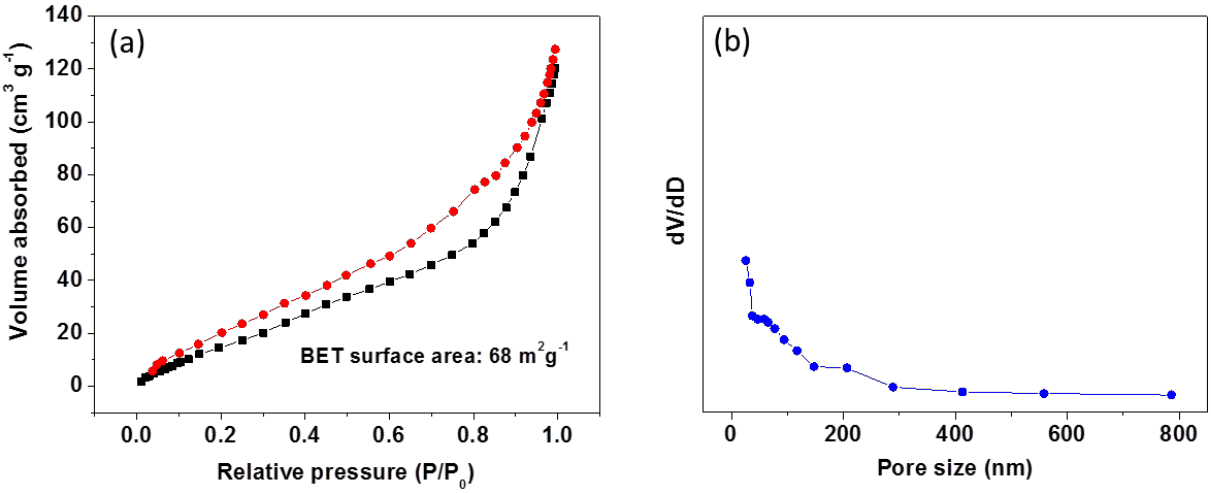

Figure S11. (a) N_2 adsorption isotherm and (b) the corresponding pore size distribution of RA-Ni_3S_2/NF

Cyclic voltammograms

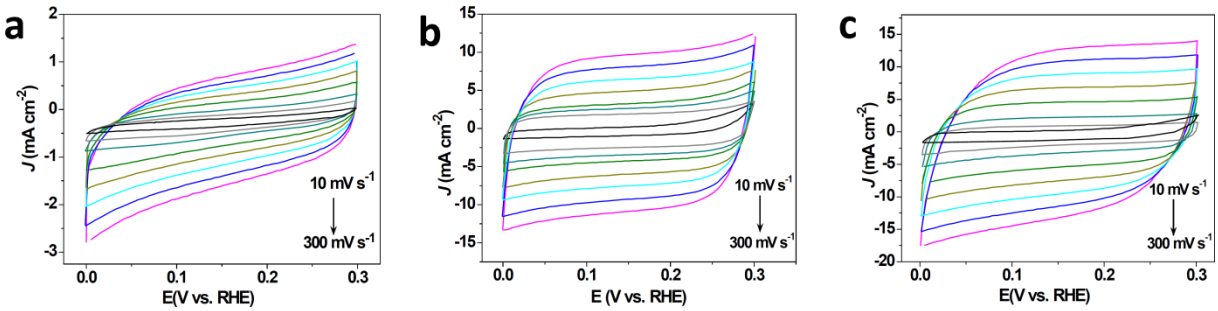

Figure S12. Cyclic voltammograms of (a) Ni foam, (b) RA-Ni_3S_2/NF, and (c) NF-Ni_3S_2/NF catalysts in the region of 0-0.3 V vs RHE.

Polarization curves normalized to their ECSA

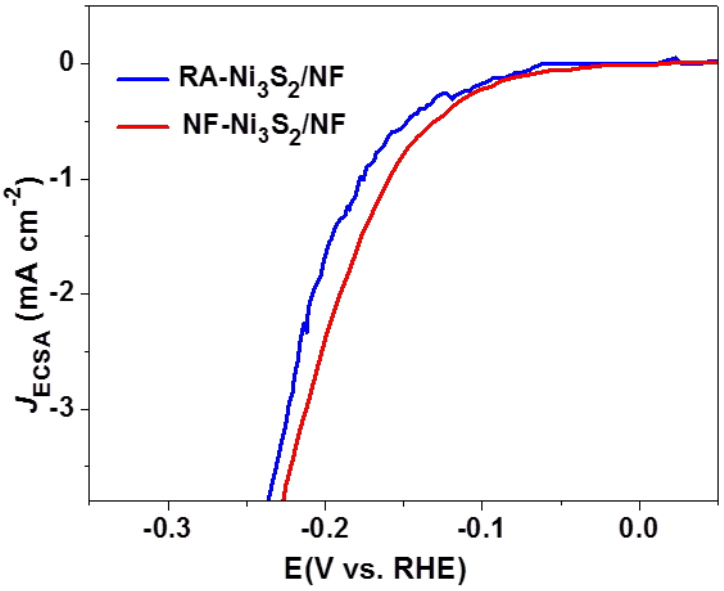

Figure S13. Polarization curves normalized to the electrochemical active surface area (ECSA) of RA-Ni_3S_2/NF, and NF-Ni_3S_2/NF catalysts in 1.0 M KOH.

Turnover frequency (TOF) values for HER and OER

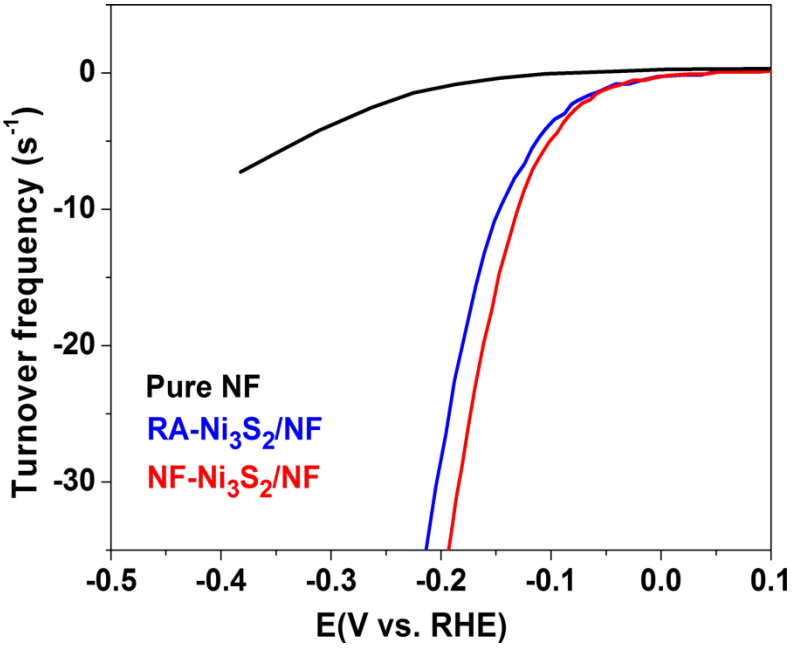

Figure S14. Calculated TOF of pure NF, RA-Ni_3S_2/NF, and NF-Ni_3S_2/NF catalysts for

HER in 1.0 M KOH solution

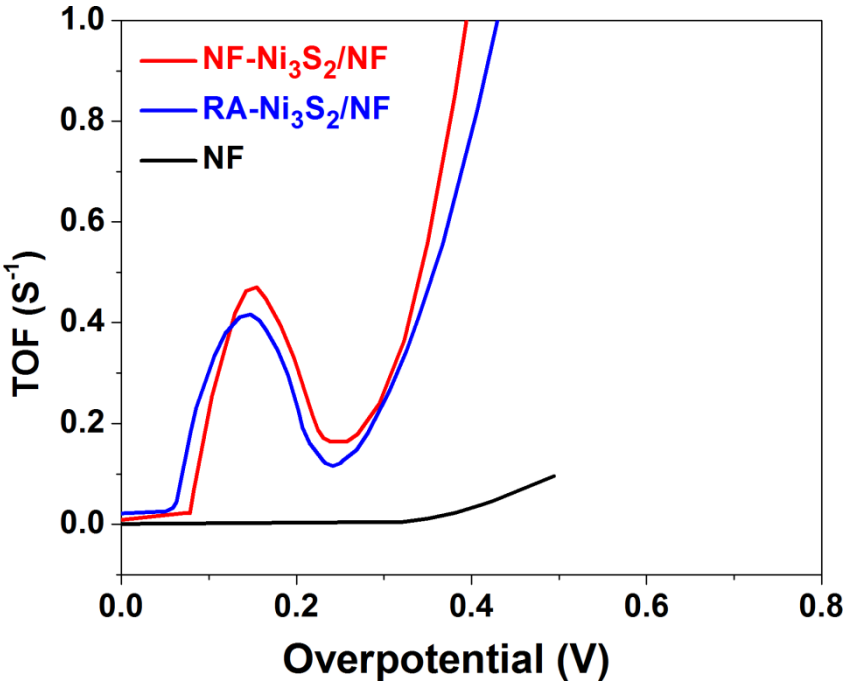

Figure S15. Calculated TOF of pure NF, RA-Ni_3S_2/NF, and NF-Ni_3S_2/NF catalysts for OER in 1.0 M KOH solution

Electrochemical impedance spectroscopy (EIS) for HER

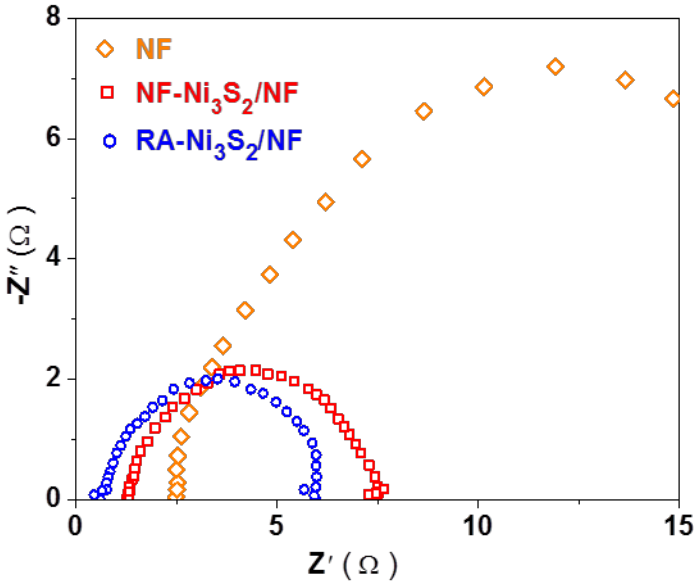

Figure S16. Nyquist plots of Pure NF, RA-Ni_3S_2/NF, and NF-Ni_3S_2/NF catalysts for HER in 1.0 M KOH.

Polarization curves normalized to their BET surface areas

Brunauer-Emmett-Teller (BET) analysis shows that the BET surface areas of Ni_3S_2 rodlike arrays and Ni_3S_2 nanoforests are 93 m^2/g and 68 m^2/g, respectively. We further display the polarization curves for HER and OER normalized to their BET surface areas. As shown in Figure S11 and S12, NF-Ni_3S_2/NF owns enhanced BET HER and OER activity over RA-Ni_3S_2/NF.

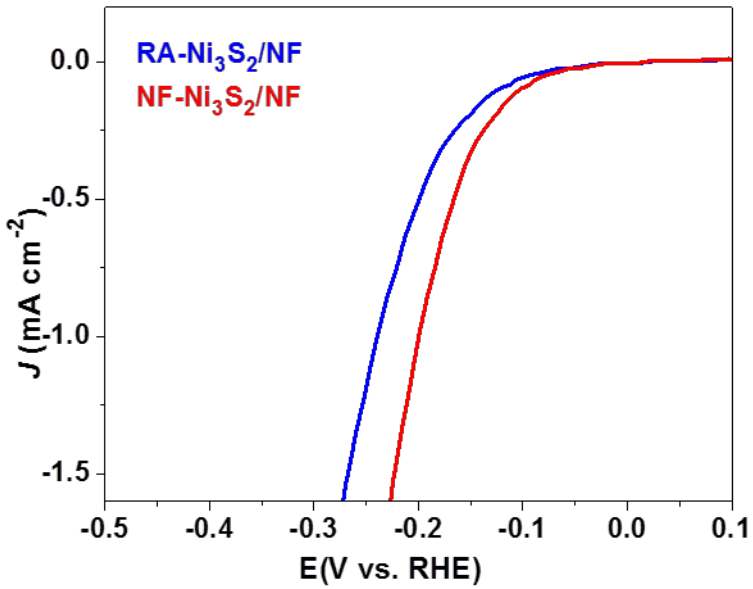

Figure S17. Polarization curves for HER of NF-Ni_3S_2/NF and RA-Ni_3S_2/NF normalized to their BET surface areas.

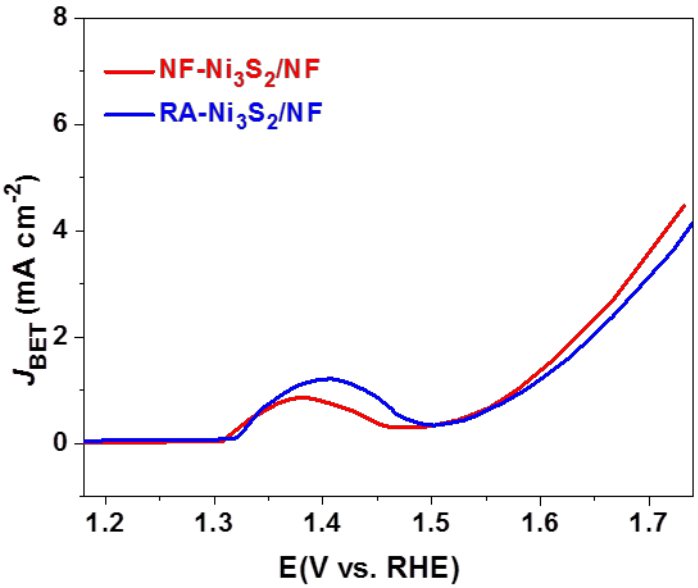

Figure S18. Polarization curves for OER of NF-Ni_3S_2/NF and RA-Ni_3S_2/NF normalized to their BET surface areas.

Characterization of catalysts after 50 h overall water splitting test

SEM images and XRD pattern (Figure S13) clearly suggest that the morphology can be remained, and the peaks of Ni_3S_2 (JCPDS 44-1418) are still clearly seen in the XRD pattern, suggesting the stability of NF-Ni_3S_2/NF and RA-Ni_3S_2/NF during the long-term overall water splitting measurement.

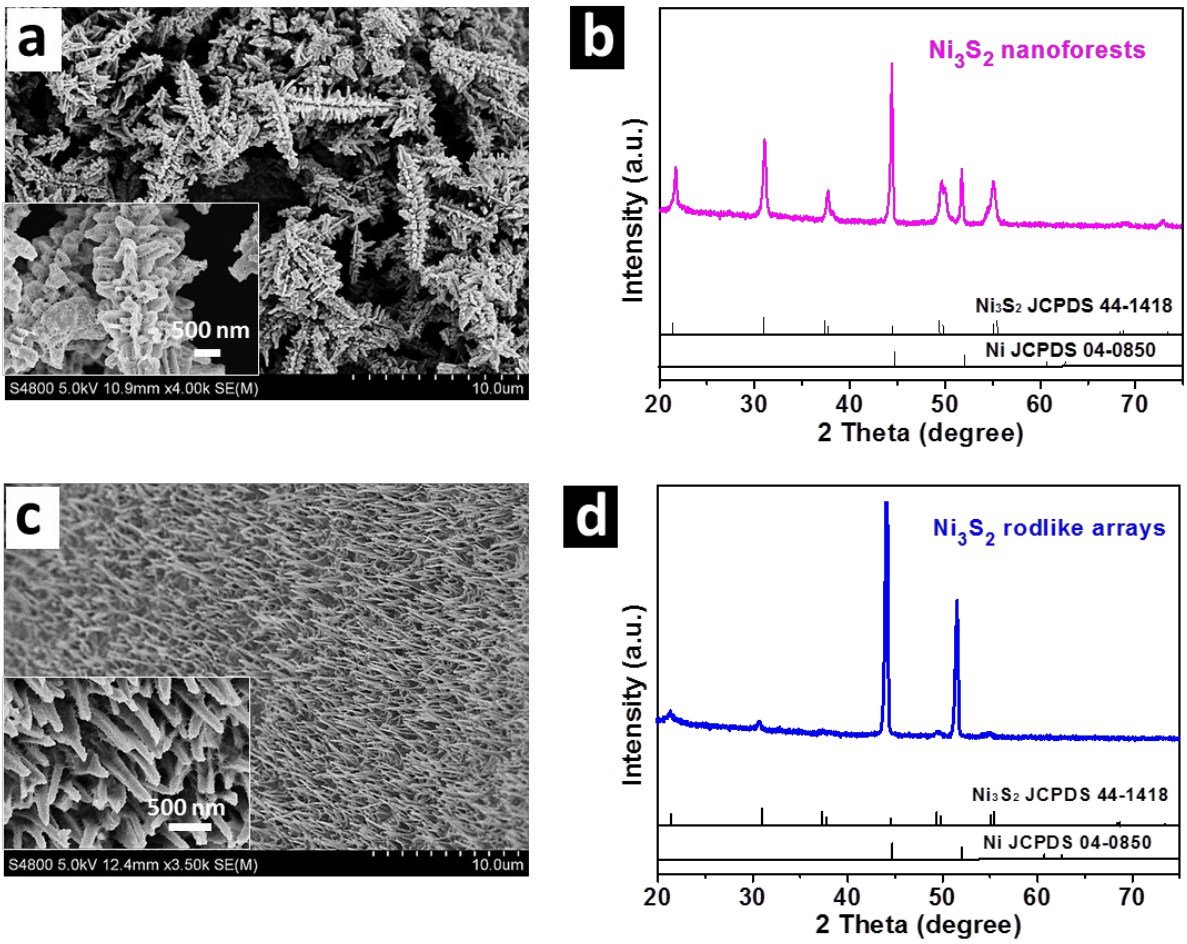

Figure S19. SEM image (a,c), XRD pattern (b,d) of RA-Ni_3S_2/NF (c,d) and NF-Ni_3S_2/NF (a,b) collected after 50 h long-term overall water splitting chronoamperometric test.

Table S1. Comparison of the OER performance of NF-Ni_3S_2/NF and RA-Ni_3S_2/NF with other reported OER electrocatalysts in basic electrolyte.

Catalysts	η10 (mV)	η_{oneset} (mV)	Tafel Slope (mV dec^{-1})	Electrolyte	Ref.
NF-Ni_3S_2/NF	220	195	59	1.0 M KOH	***This work***
RA-Ni_3S_2/NF	260	215	64	1.0 M KOH	***This work***
Ni_3S_2/Ni foam	260	-	-	1.0 M KOH	13
carbon sheets @Ni−Mn	270	250	70	1.0 M KOH	14
$(Ni, Co)_{0.85}Se$@NiCo-LDH	216	-	77	1.0 M KOH	15
NiO_x/NiOOH	320	240	58	1.0 M NaOH	16
CoNi-LDH/Fe-porphyrinlayer-by-layer	264	230	37.6	1.0 M KOH	17
nickel–iron oxide/C	310	-	42	1.0 M KOH	18
FeOOH/CeO_2 HLNTs-NF	-230	210	92	1.0 M NaOH	19
$Ni_{0.75}V_{0.25}$-LDH	350	250	50	1.0 M KOH	20
$Ni_xCo_{2x}(OH)_{6x}$@Ni	305	250	50	1.0 M KOH	21
$Ni_{45}Fe_{55}$ oxyhydroxide	310	-	65	1.0 M KOH	22
FeNi-rGO LDH	206	195	39	1.0 M KOH	23
NiFe LDHs	305	-	40	1.0 M KOH	14
$Ni_xCo_{3-x}O_4$	~620	-	66	1.0 M KOH	24
MoO_2–CoO–Carbon	270	240	37	1.0 M KOH	25
$Na_{0.08}Ni_{0.9}Fe_{0.1}O_2$	260	-	69	1.0 M KOH	17
3D-Co/cobaltphytate nanoplates	265	-	69	1.0 M KOH	18
CoCr LDH nanosheets	340	240	81	1.0 M NaOH	26
Mn-Co	320	-	52	1.0 M KOH	27
NiCoP/C	330	-	96	1.0 M KOH	28

Table S2. Comparison of overall water splitting performance of NF-Ni_3S_2/NF and RA-Ni_3S_2/NF with recently reported bi-functional electrocatalysts in basic electrolyte.

Catalysts	HER η10 (mV)	OER η10 (mV)	Overall water splitting voltage for 10 mA cm^{-2} (V)	Electrolyte	Ref.
NF-Ni_3S_2/NF	135	220	1.59	1.0 M KOH	***This work***
RA-Ni_3S_2/NF	146	260	1.62	1.0 M KOH	***This work***
NiFe nanosheets/$NiCo_2O_4$ nanoflakes/NF	105	250	1.67	1.0 M KOH	29
EG/$Co_{0.85}Se$/NiFe-LDH	260	$\frac{270\ mV}{150\ mA\ cm^{-2}}$	1.67	1.0 M KOH	30
β -$Ni(OH)_2$-OER and $NiSe_2$	184	415	~1.78	1.0 M KOH	31
carbon fiber paper (CP) @Ni-P	117	$\frac{180\ mV}{20\ mA\ cm^{-2}}$	1.63	1.0 M KOH	23
$Ni_{2.5}Co_{0.5}Fe$/NF	~150	275	1.62	1.0 M KOH	32
$Ni_xCo_{3-x}O_4$/NiCo/$NiCoO_x$	155	337	1.75	1.0 M KOH	33
Ni_3Se_2 nanoforest/Ni foam	203	$\frac{353\ mV}{100\ mA\ cm^{-2}}$	1.612	1.0 M KOH	34
Ni_xP_y-325	$\frac{160\ mV}{20\ mA\ cm^{-2}}$	320	1.57	1.0 M KOH	35
Ni-P foam	135	145	1.64	1.0 M KOH	36
V/NF	176	292	1.74	1.0 M KOH	37
Bi_2Te_3@CoNiMo on Ni foam	-	80	1.41	0.9 M KOH	35

Calculation of Faradaic efficiency

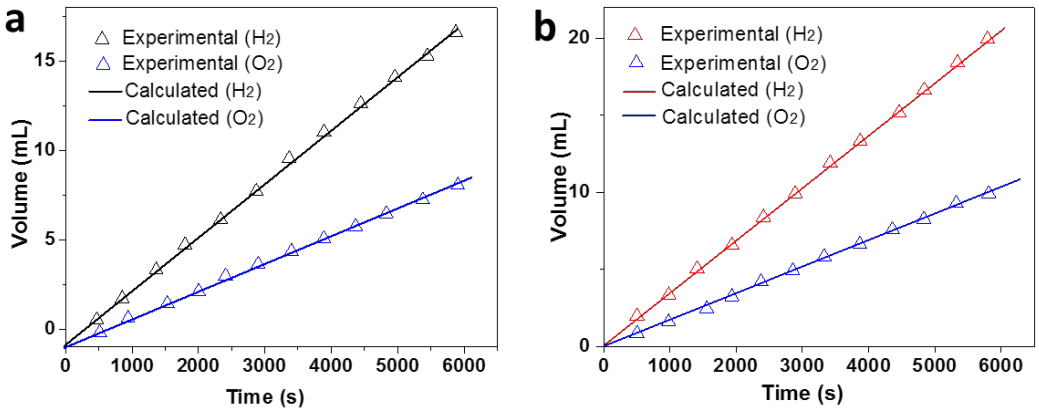

Figure S20. The amount of gas theoretically calculated and experimentally measuredversus time of overall water splitting on (a) RA-Ni_3S_2/NF and (b) NF-Ni_3S_2/NF.

References

1 Y. Wu, D. Wang, Z. Niu, P. Chen, G. Zhou and Y. Li, *Angew. Chem. Int. Ed.*, 2012, **51**, 12524-12528.

2 L. Wang and Y. Yamauchi, *J. Am. Chem. Soc.*, 2013, **135**, 16762-16765.

3 B. Qian and Z. Shen, *Langmuir*, 2005, **21**, 9007-9009.

4 H. D. Yu, Z. Zhang and M. Y. Han, *Small*, 2012, **8**, 2621-2635.

5 L. Shi, Y. Xu and Q. Li, *Cryst. Growth Des.*, 2008, **8**, 3521-3525.

6 Z. Zhang, Y. Wang, Z. Qi, W. Zhang, J. Qin and J. Frenzel, *The Journal of Physical Chemistry C*, 2009, **113**, 12629-12636.

7 Z. Zhang, X. Shao, H. Yu, Y. Wang and M. Han, *Chem. Mater.*, 2005, **17**, 332-336.

8 L. Manna, D. J. Milliron, A. Meisel, E. C. Scher and A. P. Alivisatos, *Nature Mater.*, 2003, **2**, 382-385.

9 B. Zhang, X. C. Ye, W. Dai, W. Y. Hou and Y. Xie, *Chem-Eur. J.*, 2006, **12**, 2337-2342.

10 Z. B. Zhuang, Q. Peng, J. Zhuang, X. Wang and Y. D. Li, *Chem-Eur. J.*, 2006, **12**, 211-217.

11 X. Yang, J. Zhuang, X. Li, D. Chen, G. Ouyang, Z. Mao, Y. Han, Z. He, C. Liang, M. Wu

and J. C. Yu, *Acs Nano*, 2009, **3**, 1212-1218.

12 M. Saruyama, M. Kanehara and T. Teranishi, *J. Am. Chem. Soc.*, 2010, **132**, 3280-3285.

13 L.-L. Feng, G. Yu, Y. Wu, G.-D. Li, H. Li, Y. Sun, T. Asefa, W. Chen and X. Zou, *J. Am. Chem. Soc.*, 2015, **137**, 14023-14026.

14 F. Song and X. Hu, *Nature Commun.*, 2014, **5**, 4477-4484.

15 C. Xia, Q. Jiang, C. Zhao, M. N. Hedhili and H. N. Alshareef, *Adv. Mater.*, 2016, **28**, 77-84.

16 D. A. Kuznetsov, D. V. Konev, N. y. S. Komarova, A. M. Ionov, R. N. Mozhchil and I. V. Fedyanin, *Chem. Commun.*, 2016, **52**, 9255-9258.

17 B. Weng, F. Xu, C. Wang, W. Meng, C. R. Grice and Y. Yan, *Energy Environ. Sci.*, 2017, **10**, 121-128.

18 P. Li, Z. Jin, J. Yang, Y. Jin and D. Xiao, *Chem. Mater.*, 2016, **28**, 153-161.

19 J.-X. Feng, S.-H. Ye, H. Xu, Y.-X. Tong and G.-R. Li, *Adv. Mater.*, 2016, **28**, 4698-4703.

20 K. Fan, H. Chen, Y. Ji, H. Huang, P. M. Claesson, Q. Daniel, B. Philippe, H. Rensmo, F. Li, Y. Luo and L. Sun, *Nature Commun.*, 2016, **7**, 1876-1880.

21 Z.-Q. Liu, G.-F. Chen, P.-L. Zhou, N. Li and Y.-Z. Su, *J. Power Sources*, 2016, **317**, 1-9.

22 M. Goerlin, P. Chernev, J. F. de Araujo, T. Reier, S. Dresp, B. Paul, R. Kraehnert, H. Dau and P. Strasser, *J. Am. Chem. Soc.*, 2016, **138**, 5603-5614.

23 X. Long, J. Li, S. Xiao, K. Yan, Z. Wang, H. Chen and S. Yang, *Angewandte Chemie-International Edition*, 2014, **53**, 7584-7588.

24 Y. Li, P. Hasin and Y. Wu, *Adv. Mater.*, 2010, **22**, 1926-1934.

25 B. B. Li, Q. Liang, X. J. Yang, Z. D. Cui, S. Z. Qiao, S. L. Zhu, Z. Y. Li and K. Yin, *Nanoscale*, 2015, **7**, 16704-16714.

26 C. Dong, X. Yuan, X. Wang, X. Liu, W. Dong, R. Wang, Y. Duan and F. Huang, *J. Mater. Chem. A*, 2016, **4**, 11292-11298.

27 B. Y. Guan, L. Yu and X. W. Lou, *Angewandte Chemie-International Edition*, 2017, **56**, 2386-2389.

28 P. He, X.-Y. Yu and X. W. Lou, *Angewandte Chemie-International Edition*, 2017, **56**,

3897-3900.

29 C. Xiao, Y. Li, X. Lu and C. Zhao, *Adv. Funct. Mater.*, 2016, **26**, 3515-3523.

30 Y. Hou, M. R. Lohe, J. Zhang, S. Liu, X. Zhuang and X. Feng, *Energy Environ. Sci.*, 2016, **9**, 478-483.

31 K. Fan, H. Chen, Y. Ji, H. Huang, P. M. Claesson, Q. Daniel, B. Philippe, H. Rensmo, F. Li, Y. Luo and L. Sun, *Nature Commun.*, 2016, **7**, 11981-11988.

32 X. Zhu, C. Tang, H.-F. Wang, B.-Q. Li, Q. Zhang, C. Li, C. Yang and F. Wei, *J. Mater. Chem. A*, 2016, **4**, 7245-7250.

33 X. Yan, K. Li, L. Lyu, F. Song, J. He, D. Niu, L. Liu, X. Hu and X. Chen, *Acs Appl. Mater. Inter.*, 2016, **8**, 3208-3214.

34 R. Xu, R. Wu, Y. Shi, J. Zhang and B. Zhang, *Nano Energy*, 2016, **24**, 103-110.

35 K. Yin, Z. Cui, X. Zheng, X. Yang, S. Zhu, Z. Li and Y. Liang, *J. Mater. Chem. A*, 2015, **3**, 22770-22780.

36 X. Wang, W. Li, D. Xiong and L. Liu, *J. Mater. Chem. A*, 2016, **4**, 5639-5646.

37 Y. Yu, P. Li, X. Wang, W. Gao, Z. Shen, Y. Zhu, S. Yang, W. Song and K. Ding, *Nanoscale*, 2016, **8**, 10731-10738.